DOI 10.1007/s10946-024-10216-3
Journal of Russian Laser Research, Volume 45, Number 3, May, 2024

MULTI-WAVELENGTH PASSIVELY *Q*-SWITCHED FIBER LASER BASED ON ERBIUM-DOPED FIBER SATURABLE ABSORBER AND ANALYSIS OF GAIN SATURABLE ABSORPTION CHARACTERISTICS

Honggang Pan, Rupeng Li, Chunqi Chen, Zhipan Chen,* Bo Zhang, and Zihong Zhao

Engineering Research Center of Communication Devices and Technology, Ministry of Education
Tianjin Key Laboratory of Film Electronic and Communication Devices
School of Integrated Circuit Science and Engineering, Tianjin University of Technology
Tianjin 300384, China

*Corresponding author e-mail: zhipanchen@163.com

Abstract

In this paper, we report a multi-wavelength passively *Q*-switched fiber laser based on reconfigurable Lyot ring filter (RLRF) and Erbium-doped fiber (EDF) saturable absorber (SA). The gain saturable absorption characteristics of the EDF are analyzed in the experiments. When EDF is used as SA, EDF exhibits different nonlinear characteristics at different pump powers. Through the observation of the experimental data, we discuss the relationship between the multi-wavelength and passively *Q*-switching, in view of the position of the wavelength excitations and the presence or absence of the corresponding pulse sequence. The RLRF in the structure uses a 2 m long polarization maintaining fiber (PMF), and the wavelength interval between 1.5 and 3.0 nm can be effectively switched by adjusting the polarization controller (PC). The laser elaborated can flexibly switch from a single to seven wavelengths, with a corresponding pulse repetition rates of 24.11 – 59.38 kHz, a minimum *Q*-switched pulse width of 1.16 μs, a maximum average output power of 46.98 μW, and a maximum single pulse energy of 9.64 nJ.

Keywords: multi-wavelength *Q*-switch, reconfigurable Lyot ring filter, Erbium-doped fiber, channel-spacing switch, gain saturable absorption.

1. Introduction

Multi-wavelength fiber lasers (MWFLs) have aroused the research enthusiasm of many researchers due to their advantages, such as compact structure, good stability, and superior performance in transmitting information [1]. They have extensive applications in the fields of optical fiber sensing [2, 3], optical fiber communication [4], optical detection technology, microwave photonics [5–7], and wavelength-division-multiplexing (WDM) transmission systems [8, 9]. Through the continuous efforts of scientific researchers, MWFLs have achieved rapid and stable development in recent years. In 2017, He et al. reported a tunable multi-wavelength Erbium-doped fiber laser (MWEDFL) based on a double Sagnac comb filter with PMF, which achieved a stable and tunable single, dual, and triple-wavelength laser output [10]. In 2020, Zhao et al. investigated a switchable MWEDFL based on two-mode fiber (TMF) with core-offset structure and four-wave mixing (FWM) effect, and obtained a stable six-wavelength output [3]. In 2023, Liu et al. proposed and demonstrated a switchable MWEDFL based on a taper-coupled microbottle

Manuscript submitted by the authors in English on April 24, 2024.

1071-2836/24/4503-0308

resonator, which achieves stable dual-wavelength-to-five-wavelength laser output [11]. The above laser systems are only improved in the spectra, but do not produce pulse sequences in the time domain.

In recent years, Q-switched pulses have also been developed. There are two main ways to achieve Q-switched pulse output; one is actively Q-switched and the other is passively Q-switched. Actively Q-switched pulse laser is mainly achieved by polarization modulation [12], acousto-optic modulators (AOMs) [13], electro-optic modulators (EOMs) [14, 15], rotating mirror and pumping source modulation [16]. Due to the use of these techniques, the laser structure is more complex, and the loss of the resonant cavity is greatly increased. Passively Q-switched pulse laser is mainly achieved by other materials, such as semiconductor saturation absorption mirrors (SESAMs) [17,18], single wall Carbon nanotubes (SWCNTs) [19, 20], Fe_3O_4 [21], and black Phosphorus (BP) [22], which are used as SA. However, these materials can only be used as SA. The EDF employed in our study is not only used as SA to achieve passively Q-switched pulses, but also to provide gain for the resonant cavity.

In this paper, we elaborate a multi-wavelength passively Q-switched fiber laser based on two-stage commercial Erbium–Ytterbium co-doped fiber amplifier (EYDFA) and RLRF. The EDF acts as a SA to achieve passively Q-switched pulses and exhibits different nonlinear characteristics at different pump powers. We discuss the relationship between multi-wavelength and passively Q-switched pulses in the experiments by analyzing both laser spectra and pulse sequences. The laser realizes flexible switching from a single-to-seven wavelengths, and the corresponding stable pulse sequences are achieved by adjusting the PCs.

2. Experimental Setup and Principle Analysis

2.1. Experimental Setup

In Fig. 1, we present the structure of the proposed multi-wavelength passively Q-switched fiber laser. A two-stage commercial EYDFA provides gain for the resonant cavity; the internal structure is shown in the dashed box of Fig. 1 a. Inside the EYDFA, primary pumping and secondary pumping act on the cascaded EDF and EYDF, respectively. The optical isolator (ISO) ensures unidirectional transmission of light to avoid reversing transmission of light and damaging the device. The nonlinear polarization

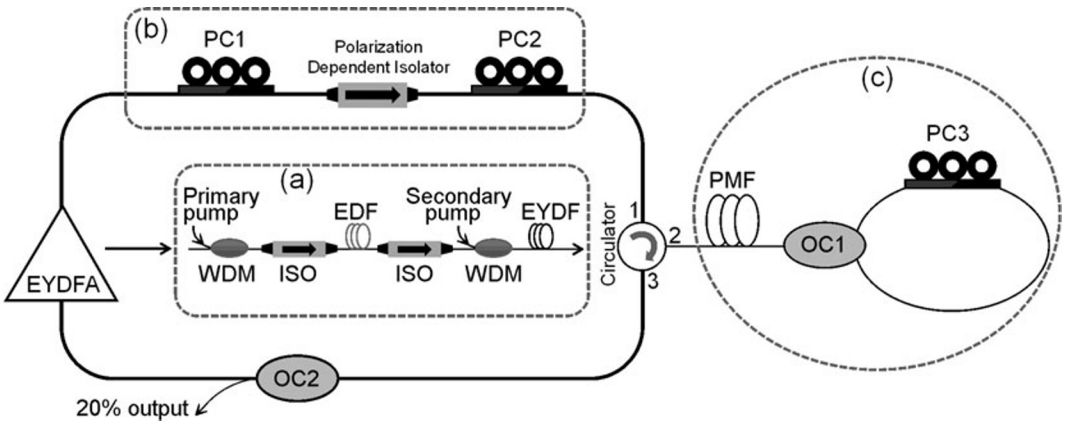

Fig. 1. Experimental setup of the laser; here, dashed box (a) is the internal structure of the EYDFA, dashed box (b) is the structure of the nonlinear polarization rotation, and dashed box (c) is the structure of the reconfigurable Lyot ring filter.

rotation (NPR) structure is shown in the dashed box of Fig. 1 b, and the intensity-dependent loss (IDL) induced by NPR can effectively suppress the mode competition in the resonant cavity, while converting the light in the laser cavity into linear polarized light. The RLRF structure is shown in the dashed box of Fig. 1 c, which mainly consists of a 2 m long PMF, a coupling ratio of 50 : 50 optical coupler (OC1), and PC3. To monitor the output light, an OC2 with a coupling ratio of 80 : 20 is used; 20% of the light is output for monitoring, and the remaining light continues to oscillate inside the cavity.

The output light is measured by an optical spectrum analyzer (OSA, YOKOGAWA AQ6370D) with a maximum resolution of 0.02 nm. The time-domain characteristics of the laser are recorded by a 200 MHz digital oscilloscope (UTD4202C) through a 200 MHz photodetector (PD-200M21391). The average output power of the laser is measured by an optical power meter (PMSII-A).

2.2. Transmission Spectrum of RLRF

First, we calculate the wavelength spacing of the comb spectrum of the standard Lyot filter, employing the following equation [23],

$$\Delta\lambda = \frac{\lambda^2}{\Delta n L}\,, \tag{1}$$

where L is the length of the PMF, λ is the central wavelength of the incident light, and Δn is the refractive-index difference between the fast axis and slow axis of PMF. The RLRF is improved on the basis of the standard Lyot filter, and the effective length of the PMF is adjusted by bidirectional propagation in the same PMF to realize the switchable wavelength interval of the comb spectrum.

In this experiment, it is assumed that the polarization state of the light passing through PC2 is at an angle of 45° to the fast axis of the PMF. When the incident light passes through PC3, the polarization state of the incident light changes; thus, the PMF effective length changes. When the angle between the polarization state of the incident light and the fast axis of the PMF after passing through PC3 is $-45°$, 0°, and 45°, the effective length of the PMF is 0, L, and $2L$, respectively. The parameters of the PMF in this experiment are $L = 2$ m, $\lambda = 1550$ nm, and $\Delta n = 4 \cdot 10^{-4}$. From Eq. (1), the constructed RLRF filter has wavelength spaces of 1.5 and 3 nm.

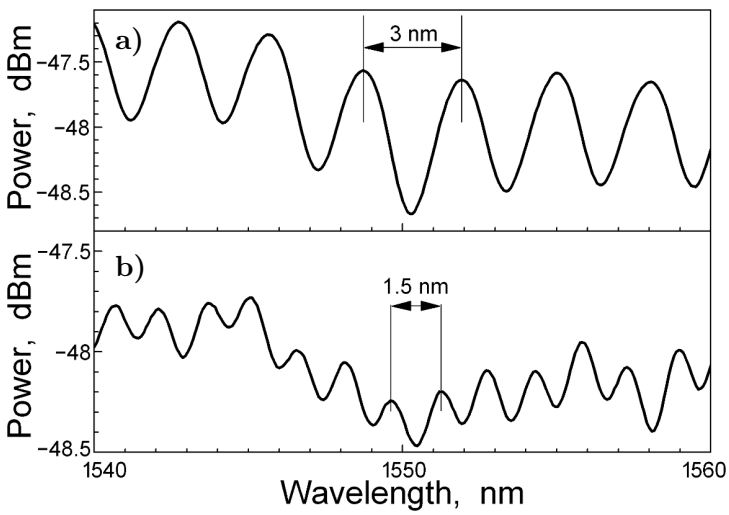

Fig. 2. Transmission spectra of RLRF in different PC3 states.

In Fig. 2, we show the experimentally measured transmission spectrum of this filter; the experimental results are consistent with the theory.

2.3. Two-Stage Commercial EYDFA Transmission Spectra

The EDF in the two-stage commercial EYDFA in the laser is weakly pumped, while the EYDF is strongly pumped. In Fig. 3, we show ASE spectra measured for the primary pump equal to 0 and a secondary pump of 200 mW, which are mainly amplified in the 1535 – 1550 nm range (the dotted curve).

Also, in Fig. 3, we show the ASE spectra measured at a primary pump power of 20 mW and a secondary pump power of 200 mW, which is mainly amplified in the range of 1535 – 1565 nm (the solid curve). It can be calculated that, when the primary pump power increases from 0 to 20 mW, the ASE spectra are mainly amplified in the wavelength range of 1550 – 1565 nm.

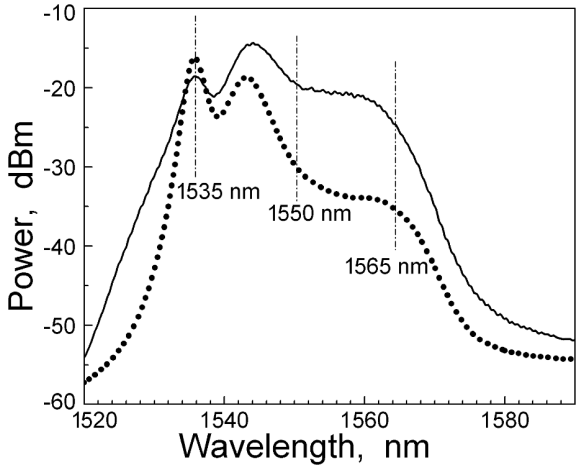

Fig. 3. ASE spectra when the primary pump power is fixed at 0 mW and the secondary pump power is fixed at 200 mW (the dotted curve) and when the primary pump power is fixed at 20 mW and the secondary pump power is fixed at 200 mW (the solid curve).

2.4. Nonlinear Characterization of EDF-SA

We investigate the nonlinear characteristics of a non-completely pumped EDF, using the average power detection by a balanced twin detector. The experimental setup is shown in Fig. 4. The input light source is a mode-locked fiber laser (MLFL) with a central wavelength of 1550 nm, a pulse duration of 240 fs, and a repetition rate of 20.457 MHz. The power of the light source can be adjusted by a variable optical attenuator (VOA). The optical power is equally distributed after passing through a 3 dB coupler. The power of one light path output is measured directly with a power meter (PM) as PM (A), and the other light path output is measured with a PM after passing through the EYDFA as PM (B). We measure the average power at points A and B with the secondary pump power fixed and the primary pump power varied.

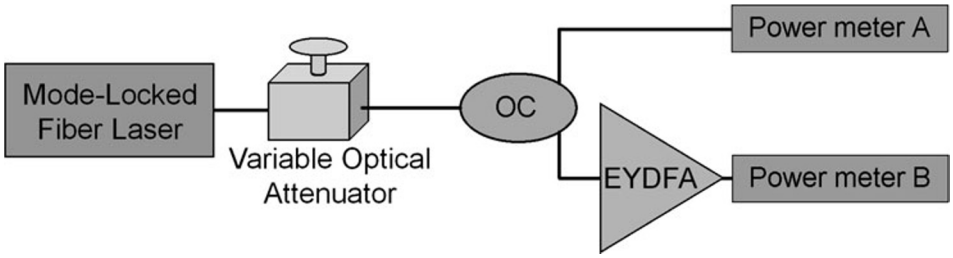

Fig. 4. Experimental device for measuring nonlinear characteristics of the EDF-SA.

In Fig. 5, we show the relationship between the input power and the output power with different primary pump powers. From the experimental results, one can see that the nonlinearity of the output power is variable with increase in the primary pump power. The output power with different pump combination is fitted by the following equation [24]:

$$I_{\text{out}} = a \cdot \exp(-I_{\text{in}}/I_{\text{sat}}) + I_0, \tag{2}$$

where the parameters a, I_{sat}, and I_0 are different for different pump combinations.

The EDF exhibits nonlinear gain characteristics under different primary pump powers, namely,

$$G \propto \frac{1}{1 + I_{\text{in}}/I_{\text{sat}}}. \tag{3}$$

In Fig. 5, we present the nonlinear characteristics of the EDF with a fixed secondary pump power at 150 mW and varied primary pump power. From the experimental results, one can see that the nonlinearity of the EDF gradually decreases with a gradual increase in the primary pump power. The nonlinearity of the EDF is the strongest at a zero primary pump power. The Q-switched pulse generation mainly depends on the nonlinear characteristics of the EDF.

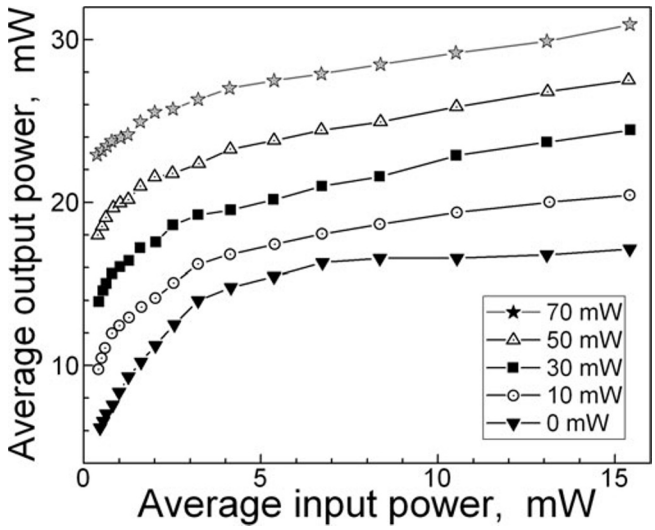

Fig. 5. The nonlinear output power with the primary pump fixed at different powers and the secondary pump power fixed at 150 mW.

3. Experimental Results and Analysis

By comparing the experimental data obtained from multiple experiments, we fix the primary pump power at 20 mW and the secondary pump power, at 200 mW, in order to obtain a better balance between the number of wavelengths and the pulse quality. We continuously adjust the PCs to get stable pulse sequences and multi-wavelength laser output. The maximum number of output wavelengths is seven wavelengths, and the pulse repetition frequency is 24.11 – 59.38 kHz. If mechanically programmable PCs is used in the experiment, more multi-wavelength lasers can be excited.

In Fig. 6 a–c, we show the single, dual, and triple-wavelength laser outputs and, in Fig. 6 a'–c', their corresponding pulse sequences are, respectively, shown. The output wavelength interval is an integer multiple of 1.5 nm, which matches the transmission spectrum. The positions of their exciting output wavelengths are in the wavelength range of 1543 – 1550 nm. In Fig. 7 a–c, we demonstrate also single, dual, and triple-wavelength laser outputs (with the corresponding time-domain waveform shown in the insets); their output wavelength excitation positions are in the wavelength range of 1550 – 1565 nm.

In Fig. 8, we show three states of different dual-wavelengths and corresponding pulse sequences obtained by continuously adjusting the PCs, with state 1 (a), state 2 (b), and state 3 (c), respectively, and the pulse sequences corresponding to the three states (a'–c'). Through observation, we find that the state 1 is similar to the laser spectrum of Fig. 6, while the state 3 is similar to the laser spectrum of Fig. 7.

In Fig. 3, one can observe that the peak power of the secondary amplification is concentrated in the wavelength range of 1535 – 1550 nm, while the peak power of the two-stage amplification is concentrated in the wavelength range of 1535 – 1565 nm. When changing the state of the PCs, the highest gain of the two-stage amplification occurs in the wavelength range of 1543 – 1550 nm due to the polarization hole burning (PHB) effect of the EDF and EYDF, defined as state 1. At state 1, the gain of the two-stage amplification is mainly provided by EYDF, and EDF serves as a SA to realize the output of the Q-switched pulse; see Fig. 8 a'. By continuously adjusting the PCs, the maximum gain of the two-stage amplification occurs in the wavelength range of 1543 – 1550 nm and 1550 – 1565 nm, respectively, defined as state 2. The EDF achieves the output of Q-switched pulses; see Fig. 8 b', and the EDF also provides gain to the laser, so its saturable absorption effect is weak.

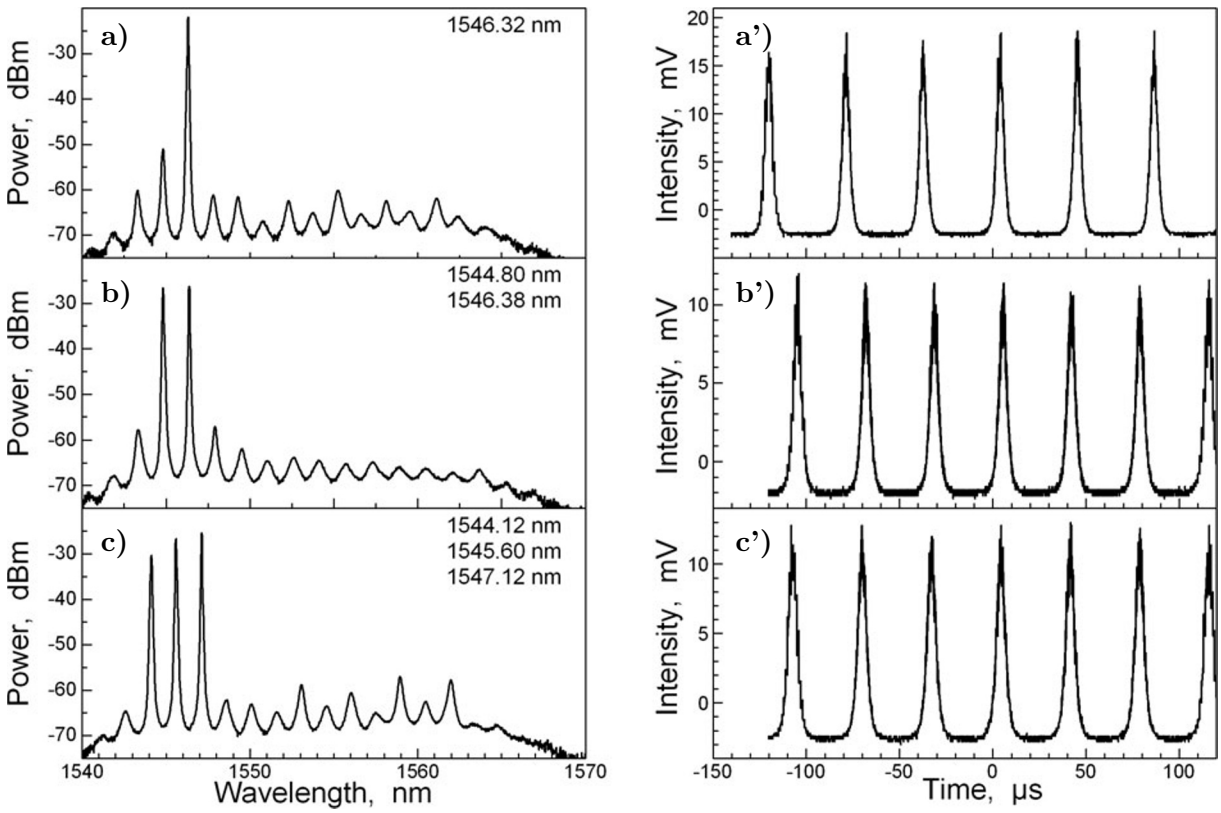

Fig. 6. Experimental results with the primary pump power fixed at 20 mW and the secondary pump power fixed at 200 mW and obtained by adjusting the PCs. Here, output spectra of the single (a), dual (b), and triple wavelength (c) and the corresponding pulse sequences (a')–(c').

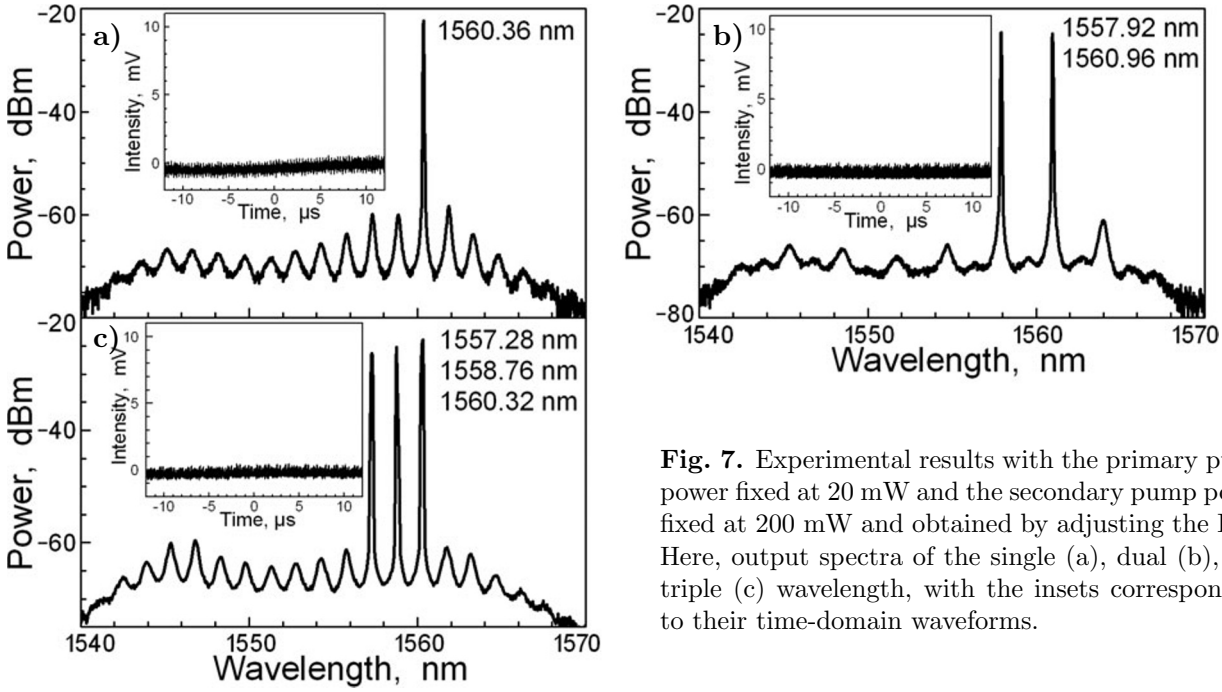

Fig. 7. Experimental results with the primary pump power fixed at 20 mW and the secondary pump power fixed at 200 mW and obtained by adjusting the PCs. Here, output spectra of the single (a), dual (b), and triple (c) wavelength, with the insets corresponding to their time-domain waveforms.

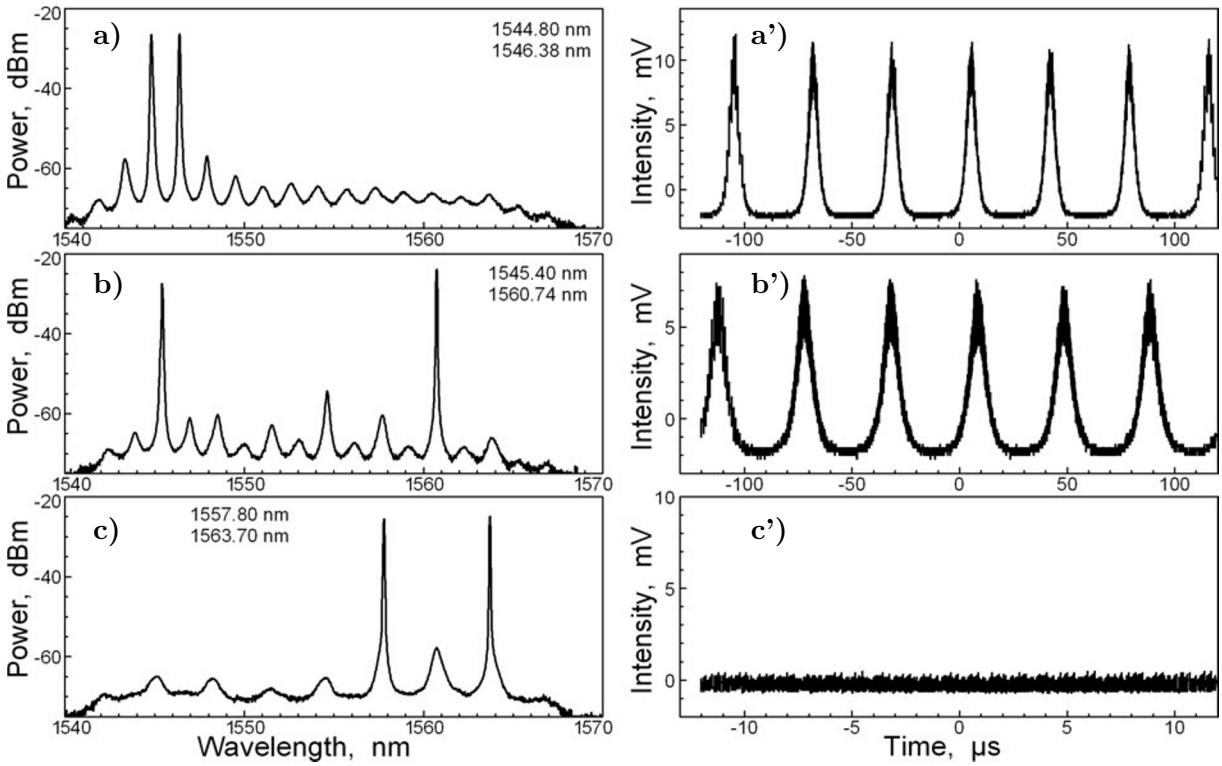

Fig. 8. Experimental results with the primary pump power fixed at 20 mW and the secondary pump power fixed at 200 mW and obtained by adjusting the PCs. Here, the output spectra of the dual-wavelength (a, b) and the corresponding pulse sequences (a', b'), with the corresponding time-domain waveform of (c) shown in (c').

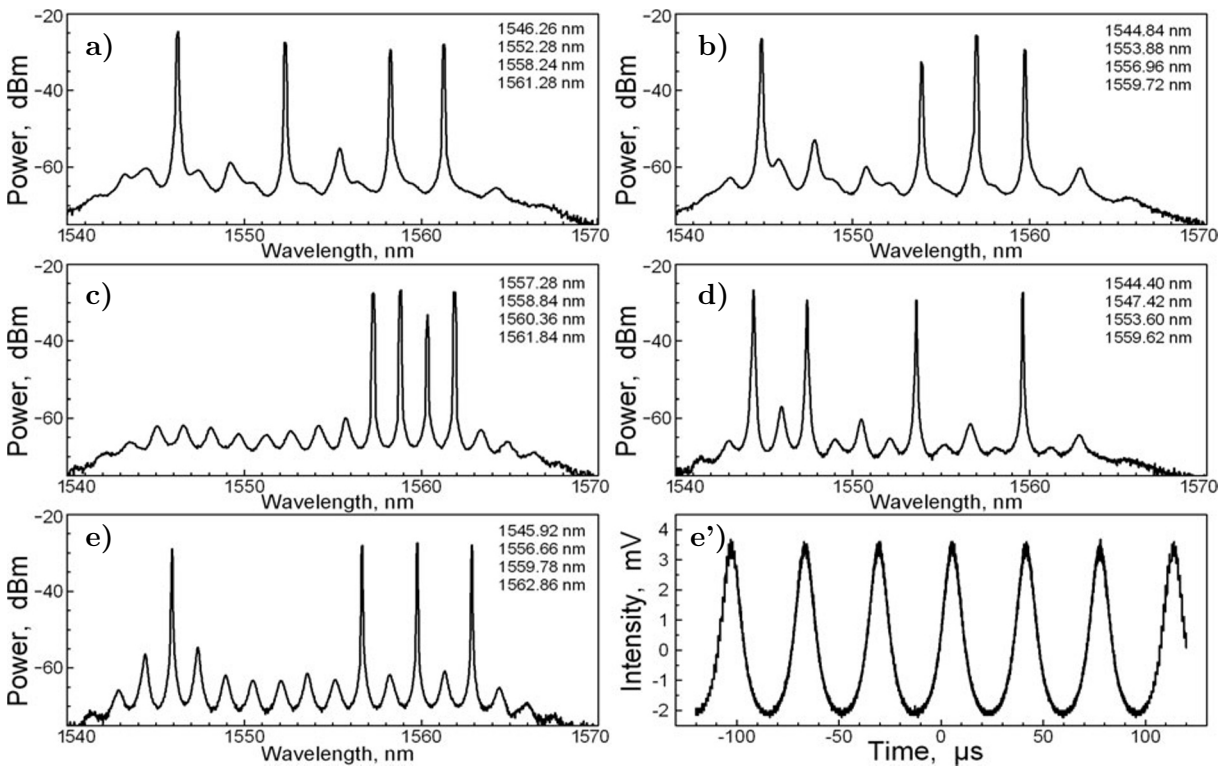

Fig. 9. Experimental results with the primary pump power fixed at 20 mW and the secondary pump power fixed at 200 mW and obtained by adjusting the PCs. Here, the output spectra of the four-wavelength (a–d) and the corresponding pulse sequences (e') of (e).

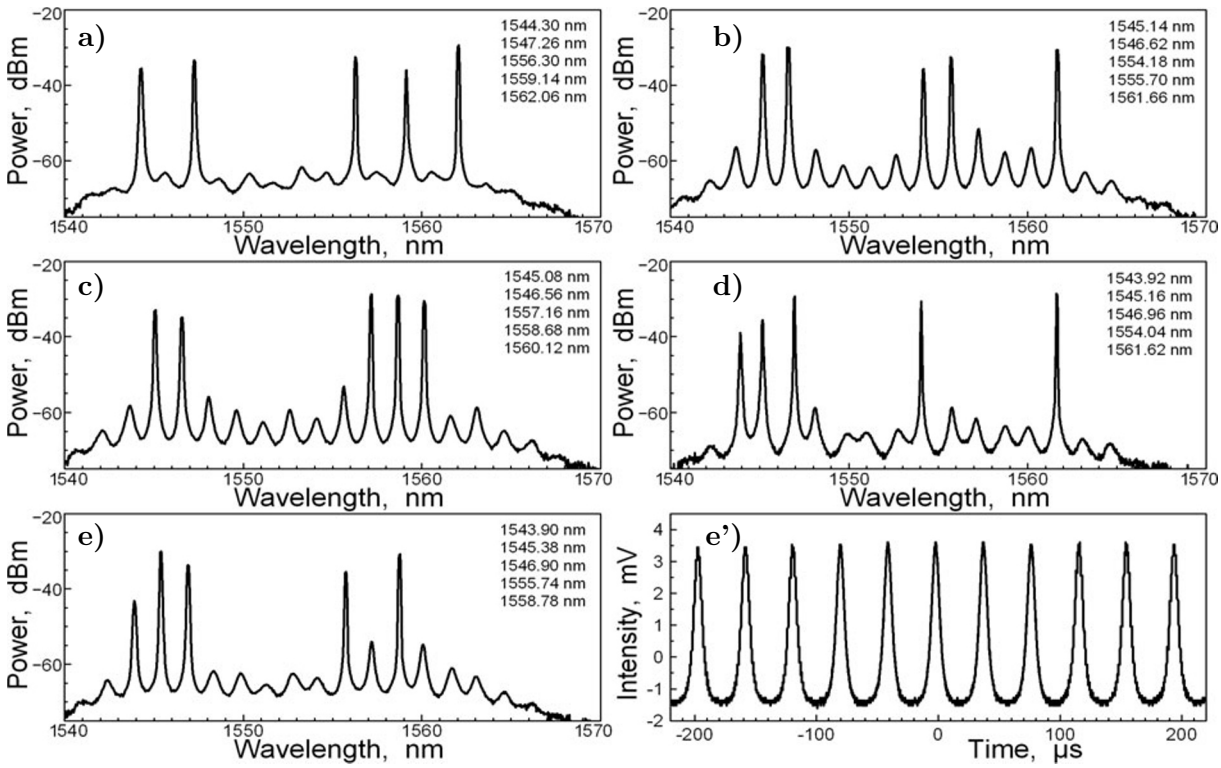

Fig. 10. Experimental results with the primary pump power fixed at 20 mW and the secondary pump power fixed at 200 mW and obtained by adjusting the PCs. Here, the output spectra of the five-wavelength (a–e) and the corresponding pulse sequences (e') of (e).

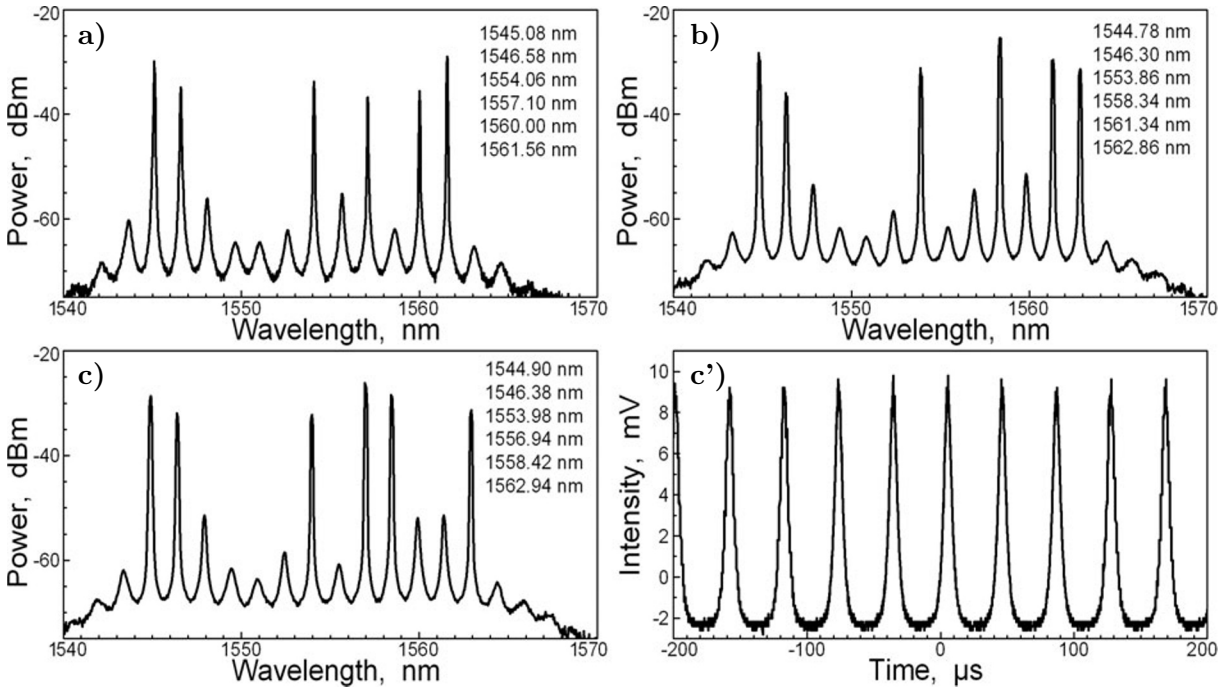

Fig. 11. The experimental results with the primary pump power fixed at 20 mW and the secondary pump power fixed at 200 mW and obtained by adjusting the PCs. Here, the output spectra of the six-wavelength (a–e) and the corresponding pulse sequences (c') of (c).

In Fig. 8 b', one can also observe that the pulse width and flatness are not as good as in Fig. 8 a'. The highest gain of two-stage amplification occurs in the wavelength range of 1550 – 1565 nm, defined as state 3. Combined with the analysis of Fig. 3, EDF in this state mainly provides gain for the laser and loses saturable absorption characteristics, so the laser output has no pulse sequences.

When the primary pump power is 20 mW and the secondary pump power is 200 mW, the laser output of four, five, six, and seven wavelengths can be obtained by appropriately adjusting the PCs; see Figs. 9–12, respectively. Each obtained laser state has a corresponding pulse sequence generated. With a gradually increase in the number of output laser wavelengths, the competition in the laser cavity becomes more and more intense, so the equilibrium of the output spectrum becomes worse and worse. From the observation of the multi-wavelength laser output position, one can see that there is no laser action in the wavelength range of 1548 – 1553 nm. One can speculate that it is difficult for a mechanical PCs to be tuned in an appropriate polarization state to produce the laser action, and the use of a programmable PCs with a monitoring mechanism may solve this problem [25, 26].

To test the stability of the laser, we record the experimental data every 10 min. in 1 h.; see Fig. 13, with the output spectrum of the laser (a) and the recorded plots of wavelength drift and power fluctuation (b).

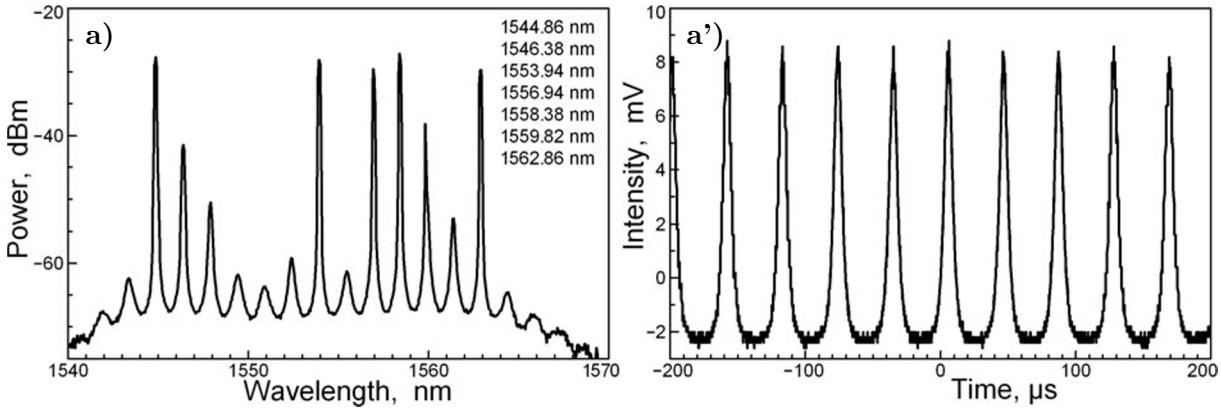

Fig. 12. Experimental results with the primary pump power fixed at 20 mW and the secondary pump power fixed at 200 mW and obtained by adjusting the PCs. Here, output spectra of the seven wavelengths (a) and the corresponding pulse sequences (a') of (a).

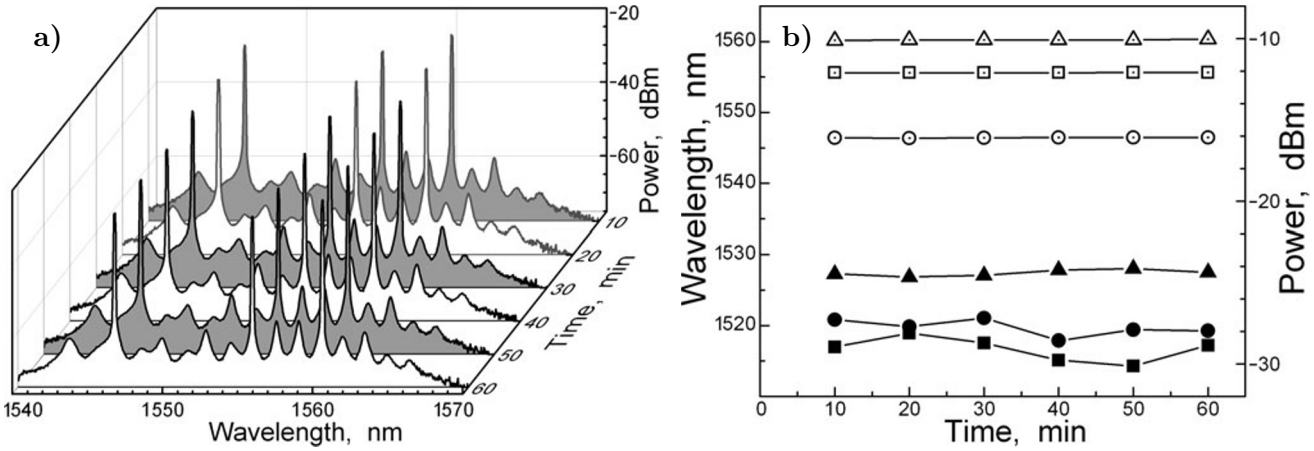

Fig. 13. Output spectra recorded every 10 min. in an hour (a) and wavelength drift (hollow markers) and power fluctuation (filled markers) of a three-wavelength laser (b).

The maximum wavelength drift is 0.08 nm, and the maximum power fluctuation is 2.063 dBm. The results show that the output spectral fluctuations of this laser are relatively small.

In Fig. 14, we show the passively Q-switched pulses generated when the PCs are fixed; also, the secondary pump power is fixed at 200 mW, and only the primary pump power varies from 0 to 55 mW. It can be clearly seen that the repetition rates of the pulse increase with increase in the primary pump power from 24.11 to 59.38 kHz, while the pulse width decreases from 5.72 to 1.16 μs. After continuing to increase the primary pump power to 70 mW, the EDF is gradually bleached, and its nonlinear absorption characteristics disappeared. The pulse sequence also disappears.

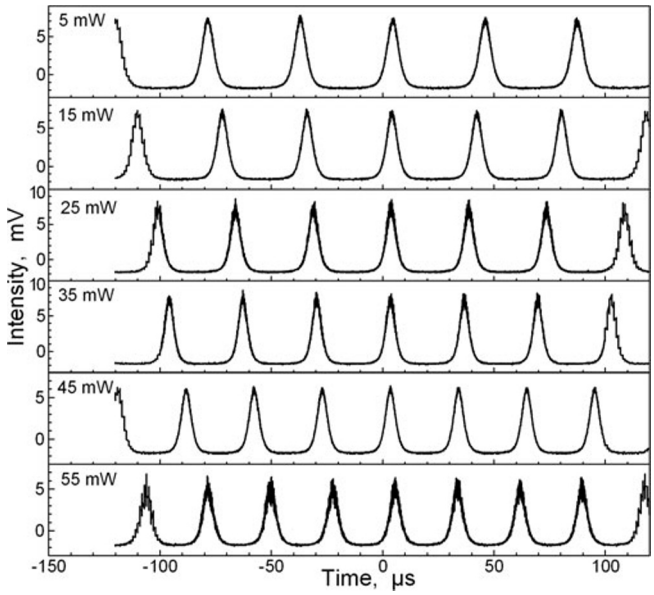

Fig. 14. Pulse sequence with the primary pump power from 5 to 55 mW, with the secondary pump fixed at 200 mW.

In Fig. 15 a, we summarize variations in the pulse repetition rate and pulse width with the pump power changing from 5 to 55 mW, with a 10 mW step. With increase in the primary pump power, the repetition rate of the pulse sequence generally shows an upward trend, while the pulse width generally shows a downward trend. When the power of the primary pump power is 45 mW, the repetition rate of the pulse rapidly rises, and the pulse width rapidly decreases. The reason is that with increase in the primary pump power, the saturable absorption effect of EDF gradually decreases, and the amplification effect becomes stronger and stronger. When the power of the primary pump is 70 mW, the EDF loses its saturable absorption effect, so the pulse sequence disappears.

In Fig. 15 b, we show variations in the average output power and single pulse energy with respect to the primary pump power. When the primary pump power increases, the average output power also gradually increases; however, the single pulse energy shows a trend of first increase and then decrease.

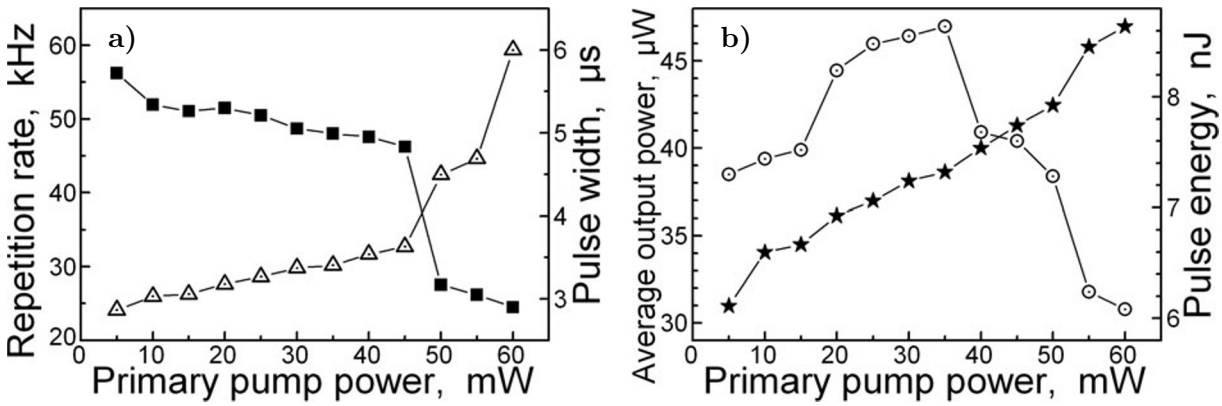

Fig. 15. Variations in the repetition rate (△) and pulse width (■) (a) and in the average output power (⋆) and pulse energy (⊙) (b) with primary pump power at a secondary pump power of 200 mW.

The single pulse energy is equal to the average power divided by the pulse repetition rate. When the primary pump power exceeds 45 mW, a rapid increase in the pulse repetition rate leads to a decrease of the pulse energy. Therefore, there is an inflection point in Fig. 15 b, and the single-pulse energy rapidly decreases as the power of the primary pump power increases.

4. Conclusions

In this study, we proposed, elaborated, and realized an all-fiber switchable multi-wavelength passively Q-switched fiber laser, using a two-stage commercial EYDFA and RLRF. We analyzed the gain saturable absorption characteristics of the EDF in the experiments. The two-stage commercial EYDFA in the structure not only provided the resonant cavity gain, but also provided the nonlinear absorption function, when the EDF was not fully pumped. When EDF was used as SA, EDF exhibited different nonlinear characteristics at different pump powers. According to the position of the wavelength excitations and the presence or absence of the corresponding pulse sequence, we discussed the relationship between multi-wavelength generation and passive Q-switching. The laser enabled flexible switching from a single wavelength to seven wavelengths and generated passively Q-switched pulses with the repetition rate of 24.11 – 59.38 kHz by adjusting the PCs.

References

1. M. F. Jaddoa, M. Z. A. Razak, M. A. M. Salim, et al., *Optik*, **127**, 8326 (2016).
2. J. Chen, Z. Tong, W. Zhang, et al., *Laser Phys.*, **28**, 055107 (2018).
3. Q. Zhao, L. Pei, M. Tang, et al., *Opt. Fiber Technol.*, **54**, 102111 (2020).
4. P. C. Peng, R. K. Shiu, M. A. Bitew, et al., *Opt. Laser Technol.*, **93**, 175 (2017).
5. Y. Dong, B. Wu, S. Xiao, et al., *Opt. Fiber Technol.*, **48**, 99 (2019).
6. S. Guo, A. Zhang, and H. Pan, *Optik*, **241**, 166973 (2021).
7. H. J. Kbashi, V. Sharma, and S. Sergeyev, *Opt. Lasers Eng.*, **137**, 106390 (2021).
8. T. Li, F. Yan, W. Han, et al., *IEEE Photonics J.*, **14**, 1 (2022).
9. T. Li, F. Yan, D. Cheng, et al., *IEEE Access*, **10**, 13026 (2022).
10. W. He, C. Shangguan, L. Zhu, et al., *Optik*, **137**, 254 (2017).
11. J. Liu, J. Liu, X. D. He, et al., *Opt. Laser Technol.*, **158**, 108819 (2023).
12. H. Wu, Z. Wang, Q. Wang, et al., *Laser Phys. Lett.*, **13**, 055101 (2016).
13. H. Wan, J. Wang, Z. Shen, et al., *Laser Phys. Lett.*, **15**, 095102 (2018).
14. A. Malinowski, K. T. Vu, K. K. Chen, et al., *Opt. Express*, **17**, 20927 (2009).
15. M. Bravo Acha, M. Fernández Vallejo, and M. López-Amo Sáinz, *Opt. Lett.*, **38**, 1542 (2013).
16. W. Shin, B. A. Yu, Y. L. Lee, et al., *Opt. Express*, **14**, 5356 (2006).
17. Z. Fang, C. Zhang, J. Liu, et al., *Opt. Laser Technol.*, **141**, 107131 (2021).
18. M. Wang, Y. J. Huang, and S. C. Ruan, *Laser Phys.*, **28**, 045103 (2018).
19. D. Sun, X. Xu, J. Chen, et al., *Opt. Laser Technol.*, **136**, 106781 (2021).
20. D. Z. Mohammed and A. H. Al-Janabi, *Laser Phys.*, **26**, 115108 (2016).
21. Y. Chen, J. Yin, H. Chen, et al., *IEEE Photonics J.*, **9**, 1 (2017).
22. C. Zhang, Y. Chen, T. Fan, et al., *Opt. Express*, **28**, 4708 (2020).
23. A. P. Luo, Z. C. Luo, and W. C. Xu, *Laser Phys. Lett.*, **6**, 598 (2009).
24. A. Zhang, C. Zhen, H. Pan, et al., *Infrared Phys. Technol.*, **131**, 104710 (2023).
25. B. Huang, X. Sheng, Z. Tang, et al., *Infrared Phys. Technol.*, **122**, 104082 (2022).
26. Y. Peng, A. Zhang, H. Pan, et al., *Opt. Laser Technol.*, **150**, 108001 (2022).